

Tunable higher-order sideband spectra in a waveguide-coupled photonic crystal molecule beyond the weak-excitation approximation

Jiahua Li,^{1,2} Rong Yu,^{3,*} and Ying Wu¹

¹*School of Physics, Huazhong University of Science and Technology, Wuhan 430074, People's Republic of China*

²*Key Laboratory of Fundamental Physical Quantities Measurement of Ministry of Education, Wuhan 430074, People's Republic of China*

³*School of Science, Hubei Province Key Laboratory of Intelligent Robot, Wuhan Institute of Technology,*

Wuhan 430073, People's Republic of China

(Received 30 August 2013; published 22 January 2014)

We investigate light transmission obtained from a hybrid optical system composed of a pair of directly coupled photonic crystal cavities called a photonic crystal molecule, a single semiconductor quantum dot, and a waveguide beyond the weak-excitation approximation. We take account of nonlinear terms in the Heisenberg-Langevin equations and give an effective method to deal with such a problem. It is shown, owing to the presence of nonlinear terms, that the efficient generation of high-order sidebands with large amplitudes can be realized with experimentally achievable system parameters. The results obtained here may be useful for gaining further insight into the properties of solid-state cavity quantum electrodynamics (CQED) system and find applications in harnessing the CQED nonlinearity to manipulate photons in a photonic crystal platform.

DOI: [10.1103/PhysRevA.89.015802](https://doi.org/10.1103/PhysRevA.89.015802)

PACS number(s): 42.50.Pq, 42.50.Ct, 42.70.Qs

Photonic crystal nanocavities are chip-based resonators which resonantly confine light to ultrasmall mode volume V with extremely low losses, giving rise to ultrahigh quality Q factor (i.e., a high Q/V ratio), greatly enhanced light-matter interaction at the nanoscale, and strong nonlinear optical response between optical fields [1,2]. In recent years, a pair of directly coupled photonic crystal cavities, also called a photonic crystal molecule (PCM), have attracted great attention in many diverse areas of research, ranging from nanophotonics [3], biochemical sensing [4], and slow light engineering [5–7] to cavity quantum electrodynamics (CQED) [8–10]. This molecular analogy stems from the observation that confined optical modes of a photonic crystal nanocavity and the electron states of atoms behave similarly. Consequently, a single photonic crystal cavity is called “photonic atom” and a pair of coupled photonic crystal cavities may be understood as a photonic analog of a molecule. Two-dimensional (2D) planar photonic crystals have emerged as an excellent device platform for realizing PCMs because of their compactness and integrability in realizing all-optical chips. Remarkably, it is also possible to deterministically couple semiconductor quantum emitters such as quantum dots (QDs) to photonic crystal cavities both spatially and spectrally in the strong-coupling regime [11]. The PCM coupled to quantum emitters forms the first step towards building a broad range of applications such as an integrated cavity network [12], quantum computing [13], and quantum simulation [14]. Some novel quantum phenomena [15–18] have been predicted experimentally and theoretically in the PCM.

In this Brief Report, we introduce a method to generate higher-order sideband spectra with a single semiconductor QD strongly coupled to a PCM beyond the weak-excitation approximation. When optical driving power is not too low and not too high (see Fig. 2 below), the weak-excitation

approximation is invalid and the nonlinear terms in the Heisenberg-Langevin equations need to be taken into account. Here, the composite system is coherently driven by an external two-tone laser field which consists of a continuous-wave control field and a nanosecond pulsed probe field and propagates through the optical waveguide. By doing fast Fourier transformation, the frequency spectral output of the temporal response, which exhibits the property of high-order sidebands, can be achieved in this coupled QD-cavity-waveguide system. The present approach is proposed in a planar photonic crystal cavity-waveguide structure that is compatible with large scale integration for the development of complex devices on a chip.

As illustrated in Fig. 1, the hybrid optical device is made up of a PCM, a two-level QD and a waveguide. Here the PCM is formed by embedding two separated point defects into a photonic crystal platform with the cavity frequency tunable by changing the geometrical parameters of the defects. The waveguide is formed by row defects in which light propagates due to the coupling between the adjacent defects. Details of the device design have been experimentally reported in detail in Refs. [8,19]. The first cavity is side coupled to the waveguide with the coupling rate κ_e . The QD with the transition frequency ω_{QD} is placed in the first cavity, and the cavity mode is coupled to the $|1\rangle \leftrightarrow |2\rangle$ transition with the coupling strength g_{cav} . Owing to the finite overlap of cavity photonic wave functions, two cavities with resonance frequencies ω_{a1} and ω_{a2} can directly couple with photon-hopping strength J which can be efficiently modulated by the distance between the two cavities. This photon tunneling can be achieved using quantum channels, such as the waveguide made by a series of coupled point defects [20]. Using the 2D planar photonic crystal structure, the initial input two-tone laser field, which includes a continuous-wave control field and a nanosecond pulsed probe field $S_{in}(t) = s_c e^{-i\omega_c t} + s_p f(t) e^{-i\omega_p t}$, where ω_c and ω_p are the carrier frequencies, s_c and s_p are the peak amplitudes of the control and probe driving fields, $f(t)$ is the normalized probe-field envelopes, is guided by optical waveguide in the crystal plane [21–23]. Under the

*Author to whom correspondence should be addressed: yurong321@126.com

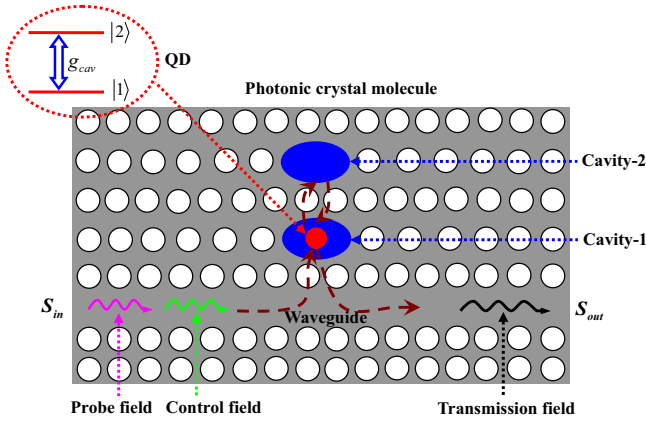


FIG. 1. (Color online) (a) Schematic illustration of the coupled system composed of a PCM, a two-level QD and a waveguide. The first microcavity containing the two-level QD is side coupled to the row defect waveguide with the coupling strength κ_e . The direct coupling of the two single-mode cavities (the coupling rate is denoted by J) can arise due to the finite overlap of their photonic wave functions. The $|1\rangle \leftrightarrow |2\rangle$ transition of QD is coupled to the mode \hat{a}_1 of the first microcavity with the coupling strength g_{cav} . A two-tone field consisting of continuous-wave control laser and Gaussian-type pulsed laser is injected into the waveguide via grating couplers [19]. S_{in} and S_{out} denote the input and the output field in the waveguide. The bubble gives energy configuration of the two-level QD and the coupling scheme of the cavity mode. $|1\rangle$ and $|2\rangle$ denote the ground and excited states of the semiconductor QD, respectively.

electric-dipole approximation (EDA) and rotating-wave approximation (RWA), the Hamiltonian describing this composite system is given in a rotating frame at the frequency of the control laser ω_c by [8,19]

$$\begin{aligned} \mathcal{H}_{rot} = & \hbar\Delta_{QD}\hat{\sigma}_{22} + \hbar\Delta_{a1}\hat{a}_1^\dagger\hat{a}_1 + \hbar\Delta_{a2}\hat{a}_2^\dagger\hat{a}_2 \\ & + \hbar J(\hat{a}_1\hat{a}_2^\dagger + \hat{a}_1^\dagger\hat{a}_2) + i\hbar g_{cav}(\hat{a}_1\hat{\sigma}_{21} - \hat{a}_1^\dagger\hat{\sigma}_{12}) \\ & + i\hbar\sqrt{\kappa_e}[s_c + s_p f(t)e^{-i\Omega t}]\hat{a}_1^\dagger - (s_c^* \\ & + s_p^* f(t)e^{i\Omega t})\hat{a}_1], \end{aligned} \quad (1)$$

where $\Delta_{QD} = \omega_{QD} - \omega_c$, $\Delta_{a1} = \omega_{a1} - \omega_c$, $\Delta_{a2} = \omega_{a2} - \omega_c$, and $\Omega = \omega_p - \omega_c$ are respectively the detunings of the QD resonance frequency ω_{QD} , the first cavity resonance frequency ω_{a1} , the second cavity resonance frequency ω_{a2} , and the frequency of the probe laser ω_p from the control laser ω_c . In the above Hamiltonian (1), $\hat{a}_{1(2)}$ and $\hat{a}_{1(2)}^\dagger$ are the bosonic annihilation and creation operators of the first (second) cavity mode. The symbols $\hat{\sigma}_{mn} = |m\rangle\langle n|$ ($m, n = 1, 2$) for $m \neq n$ are the electronic transition or projection operators between the states $|m\rangle$ and $|n\rangle$ and $\hat{\sigma}_{mm} = |m\rangle\langle m|$ ($m = 1, 2$) represent the electronic population operators involving the levels of the QD (see also the bubble of Fig. 1). s_c and $s_p f(t)$ are the field amplitudes of the two-tone driving laser propagating in the waveguide, which is directly related to the power propagating in the waveguide by $P_c^{(cw)} = \hbar\omega_c s_c^2$ and $P_p(t) = \hbar\omega_p s_p^2 f^2(t)$, respectively. In what follows, we consider that the probe driving laser is Gaussian-type pulsed field, i.e., $f(t) = \exp[-2 \ln 2(t - t_0)^2/t_p^2]$, where t_0 is the center time of the pulse, and t_p is the full width at half maximum (FWHM) of

the intensity envelope [24]. In this case, the maximum power of the driven probe pulse is $P_p^{(max)} = \hbar\omega_p s_p^2$.

The evolution of the coupled system can be described by the Heisenberg-Langevin equations. In this work, we are interested in the mean response of the coupled system, so the operators can be reduced to their expectation values. Including losses in both the cavity and QD, as well as cavity excitation, we apply the Heisenberg-Langevin formalism to attain the evolution equations as follows:

$$\begin{aligned} \frac{da_1}{dt} = & -(i\Delta_{a1} + \kappa_{i1}/2 + \kappa_e/2)a_1 - iJa_2 - g_{cav}\sigma_{12} \\ & + \sqrt{\kappa_e}[s_c + s_p f(t)e^{-i\Omega t}], \end{aligned} \quad (2)$$

$$\frac{da_2}{dt} = -(i\Delta_{a2} + \kappa_{i2}/2)a_2 - iJa_1, \quad (3)$$

$$\frac{d\sigma_z}{dt} = -\gamma_{spont}(\sigma_z + 1/2) + g_{cav}a_1^*\sigma_{12} + g_{cav}a_1\sigma_{12}^*, \quad (4)$$

$$\frac{d\sigma_{12}}{dt} = -(i\Delta_{QD} + \gamma_{spont}/2 + \gamma_{dph})\sigma_{12} - 2g_{cav}a_1\sigma_z, \quad (5)$$

with $\sigma_z = (\sigma_{22} - \sigma_{11})/2$. κ_{i1} and κ_{i2} are the cavity intrinsic decay rates, which is related to the cavity quality factor by $\kappa_{i1} = \omega_{a1}/Q_1$ and $\kappa_{i2} = \omega_{a2}/Q_2$. γ_{spont} is the QD spontaneous emission decay rate, and γ_{dph} is the QD dephasing rate, respectively. The derivation of Eqs. (4) and (5) uses the well-known mean-field (factorization) assumption $\langle \hat{A}\hat{B} \rangle = \langle \hat{A} \rangle \langle \hat{B} \rangle$ [25]. This set of coupled equations are ordinary nonlinear differential equations of complex functions instead of operators, and describe the time evolution of the coupled QD-cavity-waveguide system.

The Heisenberg-Langevin equations (2)–(5) are nonlinear, and it is very difficult to get an analytic solution to these equations. As usual, the weak-excitation approximation is adopted to deal with such a problem [26,27], where all the electrons are predominantly in the ground state of the semiconductor QD, i.e., $\sigma_{11}(t) \approx 1$ and $\sigma_{22}(t) \approx 0$ with σ_{11} and σ_{22} being the population of the QD ground and excited states. By assuming this so-called weak-excitation approximation, $\sigma_z(t) \approx -1/2$ for all time, one can substitute $\sigma_z(t)$ with its average value of $-1/2$, and thus linearize the equations. The Heisenberg-Langevin equations are reduced to a set of linear equations. Using the linearization of the Heisenberg-Langevin equations, a type of dipole-induced transparency (DIT) can be well described [27,28], which is an analog of electromagnetically induced transparency (EIT) in an atomic system [29–32]. A procedure that ignores these nonlinear terms has been commonly adopted in many previous studies [27,28,33–44]. In the present work, we take into account the nonlinear terms such as $-2g_{cav}a_1\sigma_z$, $g_{cav}a_1^*\sigma_{12}$ and $g_{cav}a_1\sigma_{12}^*$ in the above Heisenberg-Langevin equations. We find that these nonlinear terms can give rise to some interesting phenomena of the coupled QD-cavity-waveguide system, such as the efficient generation of higher-order sidebands. Concretely, the higher-order sideband processes are such that when the control laser field with frequency ω_c and the probe laser field with frequency ω_p are incident upon the photonic crystal waveguide, the

spectral components of the transmission field in Fig. 1 can be generated with frequencies $\omega_c \pm n\Omega$, where n is an integer that represents the order of the sidebands.

Now we choose the relevant experimental parameters. As noted above, the photon-hopping (or cavity-cavity hopping) strength J can be efficiently adjusted by the distance between the two cavities, so we discuss three different ranges for J , i.e., (i) the large coupling case $J \ll g_{cav}$, (ii) the competition case $J \approx g_{cav}$, and (iii) the large hopping case $J \gg g_{cav}$. For the coupled system, we set the cavity intrinsic decay rate to $\kappa_{i1}/2\pi = \kappa_{i2}/2\pi = 28$ GHz corresponding to a cavity quality factor of 11900, the coupling rate between the waveguide and cavity to be $\kappa_e/2\pi = 2.9$ GHz, and the QD spontaneous emission decay rate and dephasing rate are set to $\gamma_{spon}/2\pi = 0.16$ GHz and $\gamma_{dph}/2\pi = 5.8$ GHz, respectively. The cavity-QD coupling strength is set to $g_{cav}/2\pi = 13.4$ GHz. We also assume that the QD electron is initially populated in the ground state $|1\rangle$. All these parameters of the coupled system are chosen from a recent experiment [19], and are used throughout the work. The values of g_{cav} , κ_i and κ_e satisfy the strong-coupling condition $g_{cav} > (\kappa_i + \kappa_e)/4$, ensuring that the system operates in the strong-coupling regime.

At first, we establish the criterion when the weak-excitation approximation fails and when the nonlinear terms has to be considered. By solving Eqs. (2)–(5) numerically, Fig. 2 displays the steady-state value of the population difference σ_z as a function of optical driving power $P_c^{(cw)}$ for two different values of the QD-cavity coupling strength (a) $g_{cav} = 13.4$ GHz (strong-coupling regime) and (b) $g_{cav} = 6.7$ GHz (weak-coupling regime) when $P_p^{(max)} = 0$. It is clearly shown that the steady state is bistable and the dashed (solid) line in Fig. 2 indicates the unstable (stable) solutions. Whether or not the

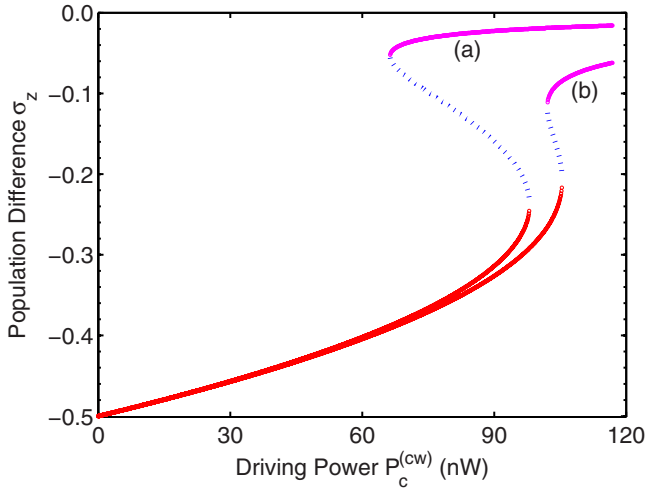


FIG. 2. (Color online) Population difference σ_z as a function of optical driving power $P_c^{(cw)}$ for two different values of the QD-cavity coupling strength: (a) $g_{cav} = 13.4$ GHz (strong-coupling regime) and (b) $g_{cav} = 6.7$ GHz (weak-coupling regime). The solid and dotted lines correspond to the stable and unstable branches, respectively. The other system parameters for simulation are chosen as $P_p^{(max)} = 0$, $J/2\pi = 1$ GHz, $\kappa_{i1}/2\pi = \kappa_{i2}/2\pi = 28$ GHz, $\kappa_e/2\pi = 2.9$ GHz, $\gamma_{spon}/2\pi = 0.16$ GHz, $\gamma_{dph}/2\pi = 5.8$ GHz, $\Delta_{QD}/2\pi = \Delta_{a1}/2\pi = \Delta_{a2}/2\pi = 0$, respectively.

QD-cavity coupling condition is strong, increasing the driving power $P_c^{(cw)}$ in Fig. 2 results in a prominent change of the population difference σ_z of the QD. From the figure we can also note that the value of the population difference σ_z is confined between $-1/2$ and 0. For the case of low excitation power, the approximation $\sigma_z \approx -1/2$ is valid for both the strong- and weak-coupling regimes between QD and cavity. In this case, the nonlinear nature of the QD can be neglected safely. Therefore, at low excitation power this approximation matches the actual output quantitatively and successfully explains a lot of theoretical and experimental observations in a linear regime. However, with increasing the driving power $P_c^{(cw)}$, this model fails completely, as the approximation $\sigma_z \approx -1/2$ becomes invalid. For sufficiently high driving power, however, one can approximate $\sigma_z \rightarrow 0$. Generally the QD is saturated and Eq. (5) reduces to $d\sigma_{12}/dt = -(i\Delta_{QD} + \gamma_{spon}/2 + \gamma_{dph})\sigma_{12}$. In view of these factors, one needs to retain the dynamics of the σ_z term in the Heisenberg-Langevin equation when the driving power is not too low and not too high.

The output field $S_{out}(t)$ can be obtained by using the input-output relation $S_{out}(t) = S_{in}(t) + \sqrt{\kappa_e}a_1(t)$ [45,46]. Equations (2)–(5) are very difficult to solve analytically for S_{out} . The output spectra can be numerically obtained by performing fast Fourier transform of $S_{out}(t)$, i.e., $S(\omega) = |\int_{-\infty}^{\infty} S_{out}(t)e^{-i\omega t} dt|$, where ω is the spectrometer frequency. Before passing to the results of the numerical calculation, it should be noted that the spectra obtained a shift for a frequency ω_c , because the Heisenberg-Langevin equations describe the evolution of the optical field in a frame rotating at the frequency ω_c . With regard to the fast Fourier transform, there are positive frequencies and negative frequencies. If the data are real, then both positive and negative frequencies have the same amplitude. If the data are complex, then positive and negative frequencies have different amplitudes [47].

Figure 3 shows the frequency spectral output of the transmission field in the coupled QD-cavity-waveguide system for three different values of J . First, we consider the large coupling case, i.e., $J/2\pi = 1$ GHz in Fig. 3(a). As shown in figure, the higher-order sidebands can be generated in the transmitted frequency spectra. For positive frequencies, the amplitude of the second-order sideband is smaller, more than one order of magnitude, than the amplitude of the first-order sideband. As the sideband order is further increased, the amplitude of the higher-order sidebands is almost kept unchanged. For negative frequencies, as can be seen from Fig. 3(a), the amplitude of the higher-order sidebands is decreased slowly when the sideband order is increased gradually. Second, with increasing J , e.g., $J/2\pi = 20$ GHz in Fig. 3(b) corresponding to the competition case, the first-order positive and negative sidebands are similar to Fig. 3(a). As compared with Fig. 3(a), the amplitudes of second-order to seventh-order sidebands for positive frequencies are enhanced. Moreover, the amplitude of other higher-order sidebands for both positive and negative frequencies is decreased obviously when the sideband order is increased. Last, for the large hopping case, i.e., $J/2\pi = 80$ GHz in Fig. 3(c), as the sideband order is increased, the amplitude of the higher-order sidebands for both positive and negative frequencies is decreased rapidly. The maximum order of the sidebands is only up to 8.

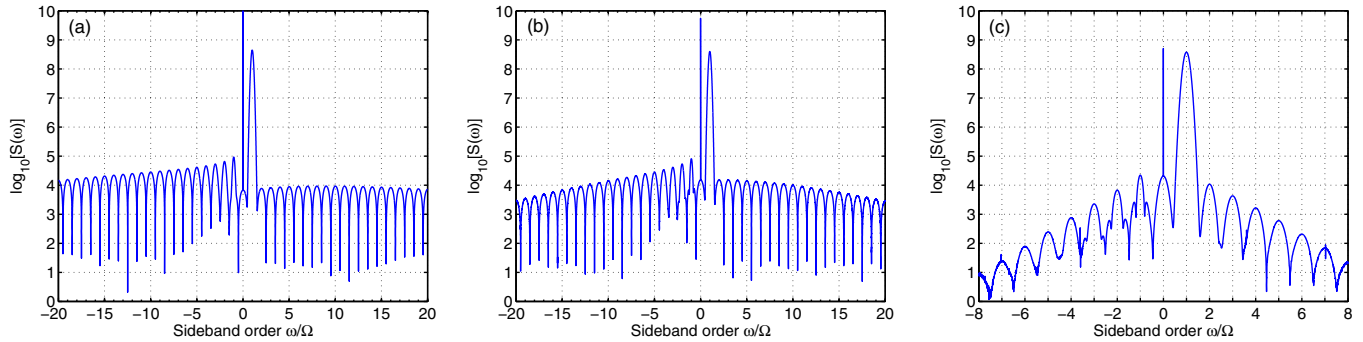


FIG. 3. (Color online) Frequency spectral output from the photonic-crystal system of Fig. 1 with a two-tone laser beam incident on the waveguide for three different values of J : (a) $J/2\pi = 1$ GHz, (b) $J/2\pi = 20$ GHz, and (c) $J/2\pi = 80$ GHz. The other system parameters for simulation are chosen as $P_c^{(cw)} = P_p^{(max)} = 90.2$ nW, $g_{cav}/2\pi = 13.4$ GHz, $\kappa_{i1}/2\pi = \kappa_{i2}/2\pi = 28$ GHz, $\kappa_e/2\pi = 2.9$ GHz, $\gamma_{spont}/2\pi = 0.16$ GHz, $\gamma_{dph}/2\pi = 5.8$ GHz, $\Omega/2\pi = 50$ MHz, $\Delta_{QD}/2\pi = \Delta_{a1}/2\pi = \Delta_{a2}/2\pi = 0$, $t_p = 50$ ns, and $t_0 = 4$ μ s, respectively.

The phenomenon above is the result of the intricate competition and balance including two kinds of the couplings, i.e., the cavity-cavity hopping J and the QD-cavity coupling g_{cav} . J as the coupling strength of the two modes indirectly influences the coupling strength of the QD with the cavity mode. In the large coupling case $J \approx 0.07g_{cav}$, the whole system can be considered as two identical Jaynes-Cummings model (JCM) subsystems weakly interacting with each other. As a result, a lot of high-order sidebands can be obtained and the corresponding amplitudes are large. In the opposite case, for large hopping $J \approx 6g_{cav}$, the photon tunneling, i.e., the excitation-transfer between two subsystems, dominates the evolution process. So only a few order sidebands appear and the amplitude of the higher-order sidebands for both positive and negative frequencies is decreased quickly.

Before ending, it is worth emphasizing that high-order sidebands shown in Fig. 3 are clearly narrow and resolved, which can be described by the uncertainty relation of time and frequency. According to the uncertainty relation of time and frequency, it is straightforward to calculate the uncertainty of the frequency as $\Delta\omega \sim 2\pi/\Delta t$. Here, the pulse lasts about $2t_p$, so $\Delta t \approx 2t_p$. Making good use of the relationships $2t_p\Omega/2\pi \sim 5$, we can arrive at $\Delta\omega \sim \Omega/5$. As a result, the high-order sideband generation is relatively narrow and resolved.

In conclusion, we have theoretically explored optical nonlinear transmission characteristics of a waveguide-coupled photonic crystal molecule embedding a two-level semiconductor QD in the strong-coupling regime. The system is driven by an external two-tone laser field (not too low and not too high), so the weak-excitation approximation is invalid and the nonlinear terms in the Heisenberg-Langevin equations need to be taken into account. By doing fast Fourier transformation, the frequency spectral output of the temporal response can be achieved in such a hybrid optical system. The results clearly show that robust high-order sidebands with large amplitudes can be generated efficiently with experimentally available system parameters. This investigation may provide further insight into the understanding of solid-state cavity quantum electrodynamics system and find applications in chip-scale high-speed optical communications in a photonic crystal platform.

This research was supported by the National Basic Research Program of China (Contract No. 2012CB922103) and the National Natural Science Foundation of China (Grants No. 11375067, No. 11275074, and No. 11104210). J.L. gratefully acknowledges Xiaoxue Yang for useful advice and discussion.

- [1] K. J. Vahala, *Nature (London)* **424**, 839 (2003).
- [2] K. J. Vahala, *Optical Microcavities* (World Scientific, Hackensack, NJ, 2004).
- [3] D. K. Armani, T. J. Kippenberg, S. M. Spillane, and K. J. Vahala, *Nature (London)* **421**, 925 (2003).
- [4] D. Dai, *Opt. Express* **17**, 23817 (2009).
- [5] X. Yang, M. Yu, D. L. Kwong, and C. W. Wong, *Phys. Rev. Lett.* **102**, 173902 (2009).
- [6] S. Kocaman, X. Yang, J. F. McMillan, M. B. Yu, D. L. Kwong, and C. W. Wong, *Appl. Phys. Lett.* **96**, 221111 (2010).
- [7] T. Gu, S. Kocaman, X. Yang, J. F. McMillan, M. B. Yu, G. Q. Lo, D. L. Kwong, and C. W. Wong, *Appl. Phys. Lett.* **98**, 121103 (2011).
- [8] A. Majumdar, A. Rundquist, M. Bajcsy, and J. Vučković, *Phys. Rev. B* **86**, 045315 (2012).
- [9] T. Cai, R. Bose, G. S. Solomon, and E. Waks, *App. Phys. Lett.* **102**, 141118 (2013).
- [10] H. Altug, D. Englund, and J. Vučković, *Nat. Phys.* **2**, 484 (2006).
- [11] K. Hennessy, A. Badolato, M. Winger, D. Gerace, M. Atature, S. Gulde, S. Falt, E. L. Hu, and A. Imamoglu, *Nature (London)* **445**, 896 (2007).
- [12] H. J. Kimble, *Nature (London)* **453**, 1023 (2008).
- [13] C. H. Su, A. D. Greentree, W. J. Munro, K. Nemoto, and L. C. L. Hollenberg, *Phys. Rev. A* **78**, 062336 (2008).
- [14] A. D. Greentree, C. Tahan, J. H. Cole, and L. C. L. Hollenberg, *Nat. Phys.* **2**, 856 (2006).
- [15] A. Dousse, J. Suffczyński, A. Beveratos, O. Krebs, A. Lemaître, I. Sagnes, J. Bloch, P. Voisin, and P. Senellart, *Nature (London)* **466**, 217 (2010).
- [16] A. A. Houck, H. E. Türeci, and J. Koch, *Nat. Phys.* **8**, 292 (2012).
- [17] K. A. Atlasov, A. Rudra, B. Dwir, and E. Kapon, *Opt. Express* **19**, 2619 (2011).

- [18] N. Caselli, F. Intonti, F. Riboli, A. Vinattieri, D. Gerace, L. Balet, L. H. Li, M. Francardi, A. Gerardino, A. Fiore, and M. Gurioli, *Phys. Rev. B* **86**, 035133 (2012).
- [19] R. Bose, D. Sridharan, H. Kim, G. S. Solomon, and E. Waks, *Phys. Rev. Lett.* **108**, 227402 (2012).
- [20] H. T. Tan, W. M. Zhang, and G. X. Li, *Phys. Rev. A* **83**, 062310 (2011).
- [21] J. Pan, S. Sandhu, Y. Huo, N. Stuhmann, M. L. Povinelli, J. S. Harris, M. M. Fejer, and S. Fan, *Phys. Rev. B* **81**, 041101(R) (2010).
- [22] J. Pan, Y. Huo, S. Sandhu, N. Stuhmann, M. L. Povinelli, J. S. Harris, M. M. Fejer, and S. Fan, *Appl. Phys. Lett.* **97**, 101102 (2010).
- [23] Y. Huo, S. Sandhu, J. Pan, N. Stuhmann, M. L. Povinelli, J. M. Kahn, J. S. Harris, M. M. Fejer, and S. Fan, *Opt. Lett.* **36**, 1482 (2011).
- [24] A. Faraon, A. Majumdar, and J. Vučković, *Phys. Rev. A* **81**, 033838 (2010).
- [25] G. S. Agarwal and S. Huang, *Phys. Rev. A* **81**, 041803(R) (2010).
- [26] S. Fan, Ş. E. Kocabaş, and J. T. Shen, *Phys. Rev. A* **82**, 063821 (2010).
- [27] E. Waks and J. Vuckovic, *Phys. Rev. Lett.* **96**, 153601 (2006).
- [28] A. Faraon, I. Fushman, D. Englund, N. Stoltz, P. Petroff, and J. Vuckovic, *Opt. Express* **16**, 12154 (2008).
- [29] S. E. Harris, *Phys. Today* **50**(7), 36 (1997).
- [30] M. Xiao, Y. Q. Li, S. Z. Jin, and J. Gea-Banacloche, *Phys. Rev. Lett.* **74**, 666 (1995).
- [31] M. Fleischhauer, A. Imamoglu, and J. P. Marangos, *Rev. Mod. Phys.* **77**, 633 (2005).
- [32] Y. Wu and X. X. Yang, *Phys. Rev. A* **71**, 053806 (2005).
- [33] E. Waks and J. Vuckovic, *Phys. Rev. A* **73**, 041803(R) (2006).
- [34] A. Auffèves-Garnier, C. Simon, J. M. Gérard, and J. P. Poizat, *Phys. Rev. A* **75**, 053823 (2007).
- [35] L. I. Childress, J. M. Taylor, A. Sorensen, and M. D. Lukin, *Phys. Rev. A* **72**, 052330 (2005).
- [36] C. Y. Hu, W. J. Munro, and J. G. Rarity, *Phys. Rev. B* **78**, 125318 (2008).
- [37] C. Y. Hu, W. J. Munro, J. L. O'Brien, and J. G. Rarity, *Phys. Rev. B* **80**, 205326 (2009).
- [38] A. Majumdar, N. Manquest, A. Faraon, and J. Vučković, *Opt. Express* **18**, 3974 (2010).
- [39] D. Sridharan and E. Waks, *Phys. Rev. A* **78**, 052321 (2008).
- [40] Y. C. Liu, Y. F. Xiao, B. B. Li, X. F. Jiang, Y. Li, and Q. Gong, *Phys. Rev. A* **84**, 011805(R) (2011).
- [41] Q. Chen and M. Feng, *Phys. Rev. A* **82**, 052329 (2010).
- [42] J. H. An, M. Feng, and C. H. Oh, *Phys. Rev. A* **79**, 032303 (2009).
- [43] X. C. Yu, Y. C. Liu, M. Y. Yan, W. L. Jin, and Y. F. Xiao, *Phys. Rev. A* **86**, 043833 (2012).
- [44] Y. F. Xiao, Y. C. Liu, B. B. Li, Y. L. Chen, Y. Li, and Q. Gong, *Phys. Rev. A* **85**, 031805(R) (2012).
- [45] D. Walls and G. Milburn, *Quantum Optics* (Springer, Berlin, 1994).
- [46] C. W. Gardiner and P. Zoller, *Quantum Noise*, 2nd ed. (Springer-Verlag, Berlin, 1999).
- [47] G. Strang, *Introduction to Applied Mathematics* (Wellesley-Cambridge Press, Wellesley, MA, 1986).